Self-Assembly of Tetranuclear Iron(II) Compounds by a Combination of Rod- and Clamp-Shaped Bridging Units

Volker Jacob,[a] Susanne Mann,[a] Gottfried Huttner,*[a] Olaf Walter,[b] Laszlo Zsolnai,[a] Elisabeth Kaifer,[a] Peter Rutsch,[a] Peter Kircher,[a] and Eckhard Bill[c]

Dedicated to Prof. Marianne Baudler on the occasion of her 80th birthday

Keywords: Self-assembly / Tetranuclear compounds / Iron(II) complexes / *tripod* ligand / Cyanides / Dicyanomethanides

Dicyanomethanides, $[RC(CN)_2]^-$ (**1**$^-$), are bridging ligands with an angular clamp-type shape. In the *tripod*/iron(II) system, [*tripod* = $CH_3C(CH_2PPh_2)_3$], they form binuclear species with three of the clamp-type ligands bridging two iron centers. An appropriate stoichiometric mixture of the *tripod* ligand, iron(II) salts and the dicyanomethanide ligand leads to the exclusive formation of [*tripod*Fe{μ-NC–C(R)–CN}$_3$-Fe*tripod*]$^+$ (**3**$^+$). Altogether, seven constituent groups arrange themselves in this type of aggregate. The process of self-aggregation is distinctly modified by the presence of cyanide ions that may act as linear rod-type bridging ligands. Equimolar mixtures of *tripod*, iron(II) salts, dicyanomethanide ligands and cyanide form tetranuclear aggregates [{*tripod*Fe}$_3$(μ-NC–C(R)–CN}$_3${μ-CN}$_3$FeX]$^+$ (**5**$^+$). In these species, the iron centers form a trigonal-pyramidal arrangement with three octahedrally coordinated *low-spin tripod*iron(II) entities in the basal plane and a tetrahedrally coordinated *high-spin* iron(II) at the apex. The iron centers in the basal plane are connected by μ^2-bridging dicyanomethanide ligands. The apical iron center is coordinated by the N-termini of three cyano ligands, which complete the octahedral coordination of the basal *low-spin* iron(II) centers. The fourth, external ligand X at the tetrahedrally coordinated *high-spin* iron(II) apex can be varied, but in most cases it is found to be a terminally coordinated dicyanomethanide entity. Without counting this variable ligand X, thirteen constituent groups of four different types selectively aggregate to form the cage compounds **5**$^+$. While the dinuclear compounds **3**$^+$ are diamagnetic, the tetranuclear species **5**$^+$ have magnetic moments close to the *spin-only* value of $\mu_{s.o.}$ = 4.9 μ_B, for tetrahedral *high-spin* iron(II). The Mössbauer spectra are in agreement with the description of **5**$^+$ above, which contain three *low-spin tripod*iron(II) entities and one *high-spin* iron(II) center. The synthesis, spectroscopic data, cyclic voltammetric data, Mössbauer data and X-ray analytical data for a series of compounds of types **3**$^+$ and **5**$^+$ are presented in this paper.

Introduction

The templates *tripod*iron(II) [*tripod* = $CH_3C(CH_2PPh_2)_3$] may serve as building blocks for supramolecular aggregates. With dinitriles such as NC−CH=CH−CN, they form tetranuclear cages [(*tripod*Fe)$_4${μ-NC−CH=CH−CN}$_6$-BF_4]$^{7+}$ in which the *tripod*iron(II) entities serve to bind three nitrile functionalities at each corner of an overall tetrahedral cage, which encloses an anion in its cavity.[1] Nitrile functionalities are ideal for engaging in this type of a supramolecular aggregation process, since the binding of RCN ligands to *tripod*iron(II) templates is reversible and flexible.[2] Reversibility of metal−ligand binding is an essential prerequisite for the controlled formation of coordination oligomers.[3−7] Based on the above reasoning, the reactivity of *tripod*iron(II) templates with anionic geminal dinitriles $[RC(CN)_2]^-$ was analyzed. Neutral geminal dinitriles have been found to promote dinuclear aggregation giving [(*tripod*Fe)$_2${μ-NC−X−CN}$_3$]$^{4+}$ [X = $C(CR_2)$, $(CH_2)_2$, $(CH_2)_3$, *o*-C_6H_4].[8] Anionic dinitriles were expected to show stronger metal−ligand-bonding, which might possibly allow for the construction and stability of aggregates of higher nuclearity. A series of dinuclear and tetranuclear aggregates derived from *tripod*iron(II) and $[RC(CN)_2]^-$ is described in this paper.

Results and Discussion

Dinuclear Compounds

The anionic geminal dinitriles **1a**$^-$−**f**$^-$ [9−16] were examined with regard to their propensity to selectively form co-

	R
1a$^-$	-S(O)$_2$CH$_3$
1b$^-$	-C(O)CH$_3$
1c$^-$	-C(O)$_2$CH$_3$
1d$^-$	-CH(CN)$_2$
1e$^-$	-C(O)CN
1f$^-$	-NO

Scheme 1. Dicyanomethanide derived ligands

[a] Anorganisch-Chemisches Institut der Universität Heidelberg
Im Neuenheimer Feld 270, 69120 Heidelberg, Germany
Fax: (internat.) + 49-(0)6221/545707
E-mail: g.huttner@indi.aci.uni-heidelberg.de
[b] Institut für Technische Chemie, Bereich Chemisch-Physikalische Verfahren (ITC-CPV), Forschungszentrum Karlsruhe
P. O. Box 3640, 76021 Karlsruhe, Germany
[c] Max-Planck-Institut für Strahlenchemie,
P. O. Box 101365, 45413 Mülheim/Ruhr, Germany

  1434−1948/01/1010−2625 $ 17.50+.50/0

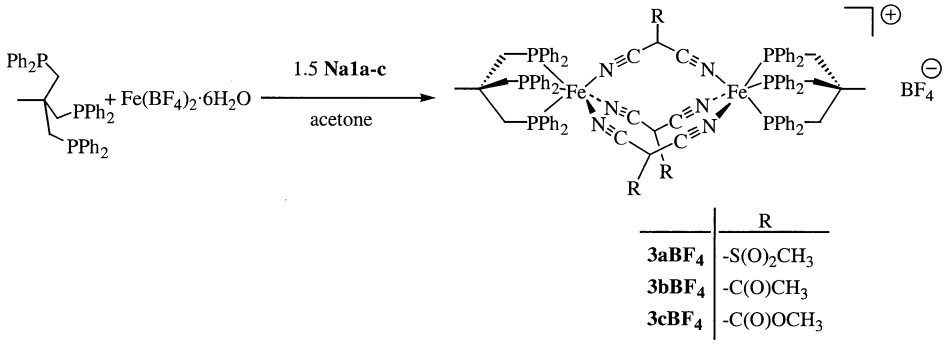

Scheme 2. Synthesis of the dinuclear compounds **3aBF$_4$**, **3bBF$_4$** and **3cBF$_4$**

ordination oligomers with *tripod*iron(II) templates (Scheme 1).

The sodium-salts of **1a**−**c**$^-$ were added to an acetone solution containing equivalent amounts of $Fe^{II}aq(BF_4)_2$ and *tripod*, in a molar ratio of 3:2 [ligand/iron(II) salt] (Scheme 2). The pale yellow solutions immediately turned red on addition of the ligands. Workup by filtration and crystallization yielded the BF_4^- salts of **3a**−**c**$^+$ as red microcrystalline solids.

Elemental analyses and mass spectra agree with the assigned constitution in each case. Coordination of the nitrile groups is evident from the observed pattern of the ν_{CN} vibrations, which are shifted to higher energies relative to the free ligands in each case (Table 2).

^{31}P NMR spectra (Table 1) show the presence of only one type of coordinated phosphorus for **3aBF$_4$**. For **3bBF$_4$**, a complicated pattern of ^{31}P NMR resonances is observed, which has not been analyzed in detail. This pattern does not change its phenotype for the temperature range 203−303 K. A rationale for this observation may be found in the assumption that the $CH_3C(O)$ substituents are not free to rotate. Conjugation within the acetyldicyanomethanido ligands will force these groups to lie within the $C(CN)_2$ planes. For the free ligand this coplanarity is evident by the observation of two ^{13}C NMR signals for the CN carbon atoms (δ = 123.9 and 121.8). One of these signals must be due to a carbon atom on the oxygen side of the acetyl substituent, and the other signal to the nitrile carbon atom at the methyl side. If the acetyl groups are in the same plane as the $C(CN)_2$ ligand entity in the coordination compound as well, and if the symmetry of the $Fe(NCCCN)_3Fe$ core is D_{3h}, there are two possible diastereomers. The statistical probability of the formation of the diastereomer, which has all three CO groups pointing to only one iron atom, is just

Table 1. ^{1}H{^{31}P}-, ^{31}P- and ^{13}C-NMR-spectroscopic data of **3BF$_4$** and **4BF$_4$** (CD_2Cl_2)

	3aBF$_4$	**3bBF$_4$**	**3cBF$_4$**	**3dBF$_4$**	**4BF$_4$**
^{1}H{^{31}P} NMR:					
tripod-CH_3	1.65 s, 6 H	1.67 s, 6 H	1.62 s, 6 H	1.79 s, 6 H	1.60 s, 6 H
tripod-CH_2	2.45 s, 12 H	2.50 s, 12 H	2.42 s, 12 H	2.55 s, 12 H	2.32 s, 12 H
ligand[a]	2.62 s, 9 H	1.52 s, 9 H	3.37 s, 9 H	2.88 s, 3 H	−
CH_{arom}	7.2−7.5 m, 60 H	7.2−7.5 m, 60 H	7.1−7.6 m, 60 H	7.2−7.8 m, 60 H	7.1−7.8 m, 60 H
^{13}C{^{1}H} NMR:					
tripod-CH_2	32.3 m	32.8 m	32.8 m	32.7 m	32.7 m
tripod-C_q	36.5 s	36.7 s	36.6 s	36.8 s	36.6 s
tripod-CH_3	37.4 m	37.6 m	37.5 m	37.0 m	37.6 m
C_{arom}	129.4−133.6	129.2−132.6	129.0−132.6	129−132.5	128.6−132.5
$C_{q,arom}$	134−136 m	134−136 m	134−136 m	135.2 dd	135.5 dd
CN[b]	−[c]	134.9[d] 135.6[d]	134.3[d] 135.0[d]	135.5 s (FeNC)	124.8 s
ligand-C_q [b]	51.7 s	−[c]	39.3 s	25.9 s	−
ligand-C[b]	47.6 s (CH_3)	191.8 s (CO) 27.6 s (CH_3)	168.8 s (COO) 51.0 s (CH_3)	113.8 s (CN) 22.3 s (CH)	−
^{31}P{^{1}H} NMR:					
PPh_2	34.8 s	31.5−39.0 m	35.4 br	38.2 s	38.8 s

[a] The ^{1}H-NMR resonances of the sodium salts of the ligands are found at δ = 2.88 (**Na1a**, [D$_6$]acetone), 1.86 (**Na1b**, [D$_6$]DMSO) and 3.51 (**Na1c**, [D$_6$]acetone). The resonance of H_2TCNE, **H1d** (CD_3NO_2), is found at δ = 5.16. − [b] The ^{13}C-NMR resonances of the sodium salts of the ligands are found at δ = 42.2 (C_q), 46.3 (CH_3) and 120.4 (CN) (**Na1a**, [D$_6$]DMSO); 26.4 (CH_3) , 47.9 (C_q), 123.9 and 121.8 (CN) and 191.0 (CO) (**Na1b**, [D$_6$]DMSO); 32.3 (C_q), 51.0 (CH_3), 123.1 and 122.0 (CN) and 168.8 (COO) (**Na1c**, [D$_6$]acetone); 119.4 s (**Na2**, [D$_6$]DMSO). The resonances of H_2TCNE, **H1d**, (CD_3NO_2) are found at δ = 26.1 (CH) and 109.1 (CN). − [c] Signal not observed. − [d] These signals interfere with signals for aromatic carbons of the *tripod* ligand.

one third of the probability of the formation of the other diastereomer, which has two CO groups pointing in the direction of one iron atom and the remaining CO group arranged in the opposite direction. In the less probable isomer all three phosphorus nuclei at each iron center are equivalent, such that a single resonance would be expected for each of the two chemically different *tripod*iron entities. In the other isomer there are two different types of phosphorus nuclei at each *tripod*iron entity, such that a doublet and a triplet resonance would be expected for each of the two different *tripod*iron entities. PP-COSY spectra show four different types of *tripod*iron entities. Due to the small differences in the chemical shifts (δ = 31.5−39) and the large coupling constants ($^2J_{PP}$ = 60 Hz), the spectrum is more complicated and has not been analyzed completely, but its general appearance is in agreement with the above hypothesis.

The ^{31}P NMR spectrum of **3cBF$_4$** shows one broad unresolved signal only, with no significant change in appearance in the temperature range from 203−303 K. With regard to the orientation of the MeOC(O) substituents relative to the coordination scaffolding, the situation is the same as discussed for **3bBF$_4$**, i.e. at least two diastereomers are expected. The coplanarity of the C(O)OR substituent with the $C(CN)_2$ part of the ligand is again evident for the free ligand from its ^{13}C NMR spectrum, which shows two different signals for the nitrile carbon atoms (δ = 123.1 and 122.0). However, in comparison with the situation in **3bBF$_4$**, the electronic differentiation between the two sides of the substituents is smaller for the methoxycarbonyl group than for the acetyl substituent. The differentiation of the chemical environment of the *tripod*iron entities by the orientation of these groups will hence be smaller for **3cBF$_4$** than for **3bBF$_4$**. This means, that the ^{31}P NMR pattern, which could still be partly resolved for **3bBF$_4$**, is no longer resolved for **3cBF$_4$** such that one broad signal is all that can be seen.

The reaction of $Fe^{II}aq(BF_4)_2$ and *tripod* with **H1d**[14] in acetone leads to the dinuclear compound **3dBF$_4$**, under spontaneous deprotonation of **H1d**.[17] Short reaction times allow for the isolation of the BF_4^- salt of **3d**$^+$ as a red microcrystalline compound, in yields of about 50% (Scheme 3).

The analytical data are in agreement with the assigned constitution (Tables 1 and 2). The ^{31}P NMR spectra (Table 1) show one sharp singlet resonance as expected for two chemically equivalent *tripod*iron(II) units. The ^{1}H NMR resonance of the dicyanomethyl substituent is found at δ = 2.88 (**3dBF$_4$**, CD_2Cl_2). With the proton signal of the neutral ligand lying at δ = 5.16 (**H1d**, CD_3NO_2), the coordination shift is remarkably high.

Sodium dicyanamide, **Na2**, also reacts in the typical way yielding the dinuclear compound **4BF$_4$** as a red violet microcrystalline material (90%) (Scheme 4).

The analytical data (Table 2) and NMR spectra (Table 1) are in agreement with the assigned constitution. The ^{13}C NMR signals of the nitrile groups shift from δ = 119.4 (**Na2**, [D$_6$]DMSO) to δ = 124.8 (**4BF$_4$**, CD_2Cl_2), on coordination (Table 1).

Crystals suitable for X-ray analysis could be grown for three compounds of the series **3BF$_4$** (**3aBF$_4$**, **3bBF$_4$**, **3dBF$_4$**). Structural analysis revealed the same principal type of coordination for all three compounds. Therefore, only the structure of **3b**$^+$ is shown in Figure 1. The structural data for all three compounds are presented (Exp. Sect., Table 5).

The $Fe(NCCCN)_3Fe$ core shows an approximate C_3 symmetry in each case (Figure 1). The distances between the iron centers are almost the same in the three compounds [Fe···Fe 692 pm (**3a**$^+$), 680 pm (**3b**$^+$), 687 pm (**3d**$^+$)]. They are determined by the geometry of the NCCCN bridging entity, which is the same in all three compounds. With almost ideal octahedral coordination at the iron centers, ligand geometry does not allow for strictly linear Fe−N−C arrangements (Figure 1). Throughout the series of the three compounds Fe−N−C angles are in the range of 157−169°. The substituents at the $C(CN)_2$ ligand constituent show no pπ−pπ conjugation with the $C(CN)_2$ unit in **3a**$^+$ and **3d**$^+$, whereas the acetyl substituent in **3b**$^+$ definitely does so. The corresponding C−C distances are only 143.7 pm in **3b**$^+$, while they are 150 pm in **3d**$^+$. This π conjugation seen in **3b**$^+$ is also evident from the strict coplanarity of all nonhydrogen atoms of each ligand in **3b**$^+$. The relevant torsion angles are around 0° and 180°, ±5°. The interpretation of the spectroscopic data for **3bBF$_4$** as given above (Table 1 and 2), is in full accord with the observed structure of **3b**$^+$, which conforms to the statistically preferred isomer with regard to the rotational position of the acetyl groups (Figure 1).

All compounds **3BF$_4$** and **4BF$_4$** show reversible one-electron oxidations to the mixed-valent Fe^{II}/Fe^{III} species. Oxidation occurs at around 1000 mV vs. SCE, with a slight variation depending on the specific type of ligand (Table 4). The lowest oxidation potential is observed for **4BF$_4$** ($E_{1/2}$ = 910 mV vs. SCE), oxidation is most difficult for **3aBF$_4$** ($E_{1/2}$ = 1120 mV vs. SCE) with its electron-withdrawing

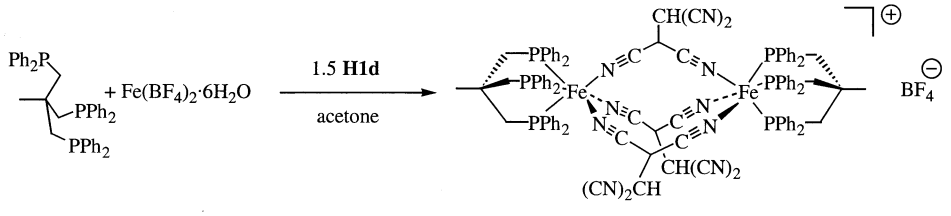

3dBF$_4$

Scheme 3. Synthesis of the dinuclear compound **3dBF$_4$**

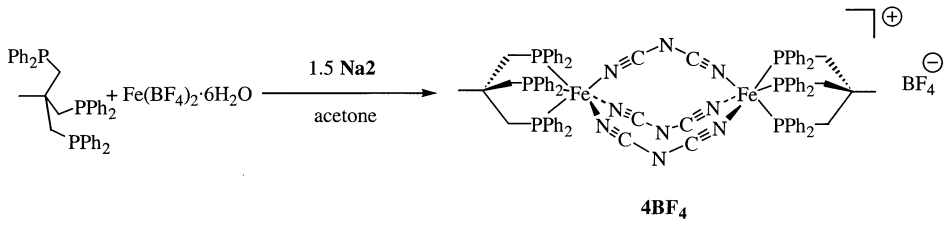

4BF$_4$

Scheme 4. Synthesis of the dinuclear compound **4BF$_4$**

Table 2. Analytical and spectroscopic data of the dinuclear compounds **3BF$_4$** and **4BF$_4$**

No.	Formula (M [g/mol])	MS m/z (%)	[Fragment]	HR-MS m/z	$M^+_{calcd.}$ M^+_{found}	C, H, N, P (calcd.) C, H, N, P (found)	IR (CsI) $\tilde{\nu}$ [cm^{-1}] ν_{CN}	$\nu_{XO,\ XO2}$
3aBF$_4$	$C_{94}H_{87}BF_4Fe_2N_6O_6S_3P_6$	1790(11)	$[M]^+$	–	–	60.12, 4.67, 4.48, 9.90	2218 sh	1323 s
	(1877.3)	823(80)	[*tripod*Fe**1a**]$^+$	–	–	59.09, 5.09, 4.30, 9.53	2200s	1137 s
3bBF$_4$	$C_{97}H_{87}BF_4Fe_2N_6O_3P_6$	1680(7)	$[M]^+$	–	–	65.86, 4.96, 4.75, 10.50	2226 sh	1628 s
	(1769.1)	1057(21)	[M − *tripod*]$^+$	–	–	65.24, 5.14, 4.80, 10.39	2204 s	1607 s
3cBF$_4$	$C_{97}H_{87}BF_4Fe_2N_6O_6P_6$	1730(11)	$[M]^+$	1729.3804	1730.3794	64.08, 4.83, 4.63, 10.23	2232 sh	1685 s
	(1817.1)	–	–	1729.3820	1730.3846	63.41, 5.10, 4.51, 10.02	2208 s	–
3dBF$_4$	$C_{100}H_{81}BF_4Fe_2N_{12}P_6$	1748(7)	$[M]^+$	–	–	65.45, 4.45, 9.16	2218 sh	–
	(1835.2)	706(100)	[*tripod*FeCN]$^+$	–	–	65.05, 4.57, 9.03	2178 vs	–
4BF$_4$	$C_{88}H_{78}BF_4Fe_2N_9P_6$	–	–	1558.3555	1559.3542	64.20, 4.78, 7.66	2298 s	–
	(1646.0)	–	–	1558.3512	1559.3538	63.45, 4.97, 7.78	2207 vs	–

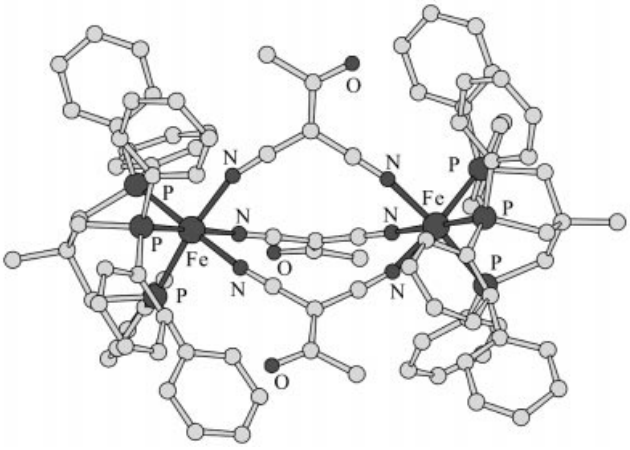

Figure 1. Crystal structure of the cation **3b$^+$**; selected bond lengths [pm] and angles [°]: Fe−P 224.3(2) to 227.9(2), Fe−N 196.8(6) to 199.0(7), C−N 112(1) to 117(1), C_{CN}−C 139(1) to 142(1), C_{CO}−C 143(1) to 144(1), C_{Me}−C_{CO} 147(1) to 151(1), C−O 123(1) to 126(1); P−Fe−P 86.7(1) to 91.0(1), N−Fe−N 82.1(2) to 84.3(2), Fe−N−C 159.3(5) to 168.9(6), N−C−C 176(1) to 179(1), C_{CN}−C−C_{CN} 114.2(6) to 116.8(6)

sulfonylmethyl substituents. A second reversible one-electron oxidation step is observed for all compounds except **3dBF$_4$** (Table 4). The separation between the first and second one-electron oxidation potential, $E_{1/2}{}^1 - E_{1/2}{}^2$, is approximately 300 mV throughout.

Tetranuclear compounds

The above results show that geminal anionic dinitriles tend to form dinuclear compounds with *tripod*iron(II) units. This cannot be a consequence of the anionic charge on the ligands, since neutral dinitriles show the same preference of forming dinuclear, triply bridged diiron compounds. Therefore, it must be a consequence of the geometry of the bridging ligands. In these dicyanomethanide derivatives, the two nitrile groups are separated by just one linker atom, thus spanning an angle between 109 and 120°. The geometry of these ligands thus differs distinctly from the one in fumaric dinitrile, where the nitrile groups are separated by two spacer atoms such that the nitrile groups are parallel to each other. Thus, with fumaric dinitrile as a bridging ligand, the ligand − including the linker entity − and the metal centers bound to it are roughly colinear (Scheme 5 **A**). However, with dicyanomethanide-type ligands, the bridging ligand and the two metal centers bound to it arrange themselves in a roughly triangular shape with the space segment along the line connecting the metals centers being empty (Scheme 5 **B**).

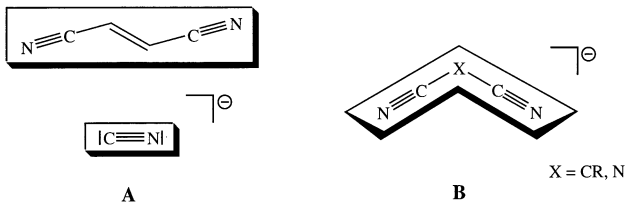

Scheme 5. Linear rod-type and triangular clamp-type bridging ligands

The main geometric difference between these two types of ligands is that fumaric dinitrile behaves as a rod-like building block, while dicyanomethanide derivatives and their analogues serve as a kind of "triangular clamp". This corresponds to the difference in behavior of these building blocks if they are used to construct oligonuclear metal com-

pounds by a self-organized process. With a linear rod-type ligand, only one ligand fits between two metal centers. With ligands forming triangular clamp-like arrangements, there is no such restriction and up to three ligands can easily be arranged to form a triply bridged dinuclear compound (e.g. **3BF$_4$** and **4BF$_4$**).

If the goal is to achieve higher nuclearity in self-arrangement processes, linear rod-type ligands would hence be the proper choice since three such ligands fixed in a monodentate way to one metal center can never ligate to another one with their other end. In fact, under conditions similar to the ones used for the preparation of compounds of the type **3BF$_4$** and **4BF$_4$** (this work), or [*tripod*Fe{μ-NC−C(CR$_2$)−CN}$_3$Fe*tripod*]$^{4+}$,[8] fumaric dinitrile yields a tetranuclear compound [(*tripod*Fe)$_4${μ-NC−CH=CH−CN}$_6$BF$_4$]$^{7+}$ [1] with a tetrahedral arrangement of the metal atoms. The opposite tendency of dicyanomethanide-derived ligands to result in triply bridged dinuclear compounds, might then be overcome in a self-organization process in which both linear rod-type ligands and triangular clamp-type species are used. This hypothesis was tested by repeating the reaction leading to **3BF$_4$** and **4BF$_4$** in the presence of varying amounts of cyanide as a linear rod-type linker (Scheme 5 **A**). It was found that tetranuclear compounds **5BF$_4$** are in fact formed with the appropriate molar ratio (Scheme 6).

When the sodium salt of **1a**$^-$ is added to a mixture of Fe^{II}aq(BF$_4$)$_2$ and *tripod* in dichloromethane/ethanol (1:1), a color change from pale yellow to red immediately occurs and up to this point the appearance of the reaction mixture is very similar to that observed in the preparation of **3a**$^+$. Solid sodium cyanide is added to this mixture. A gradual color change from red to orange-red is observed over a period of 10 h. On concentration, an orange-red material precipitates, which is purified by dissolution in dichloromethane, filtration and crystallization from dichloromethane/ethanol. Analysis of the orange microcrystalline product shows that it is **5aBF$_4$**. The ν_{CN} IR spectra show a prominent long-wavelength band at 2106 cm^{-1} (CsI) (Table 3), which is assigned to the vibration of a μ^2-bridging cyanide ligand.[18] In dichloromethane, this band is found to split into two components, which is assigned to the symmetric (A_1, 2111 cm^{-1}) and asymmetric (E, 2105 cm^{-1}) vibrations of the locally C_3-symmetric Fe(NC)$_3$ unit. This assignment is corroborated by the observation that a band at around this wavelength is present in the IR spectra of all compounds of the type **5BF$_4$**, while it is absent in the IR spectra of compounds of the type **3BF$_4$** which do not contain a bridging cyanide ligand. The ν_{CN} bands, which are characteristic of the bridging dicyanomethanide ligands in **3BF$_4$**, are found at shorter wavelengths in the range of 2180−2230 cm^{-1} (Table 2). In the tetranuclear compounds **5BF$_4$**, vibrations in the same range are hence assigned to μ^2-bridging dicyanomethanide ligands (Table 3). For **5aBF$_4$**, these bands are found at 2216 and 2184 cm^{-1}. A shoulder at 2166 cm^{-1} indicates the presence of a terminally coordinated dicyanomethanide ligand.[19,20] The shoulder observed in the CsI phase, appears as a separate band in the dichloromethane phase at 2163 cm^{-1} (Table 3). A band at this frequency (2165 ± 10 cm^{-1}) is observed for all compounds (**5aBF$_4$**, **5bBF$_4$**, **5cBF$_4$**, **6BF$_4$**) which have a geminal dinitrile coordinated as the terminal ligand to the apical iron center (Table 3). FAB$^+$ mass spectra show the signal for the parent molecular ion **5a**$^+$ at *m*/*z* = 2748. Fragments corresponding to the consecutive loss of *tripod* ligands (*m*/*z* = 2123 [M$^+$ − *tripod*], 1498 [M$^+$ − 2*tripod*]) are also observed. The Mössbauer spectrum of **5aBF$_4$** shows a pattern with four absorbance maxima, which is clearly a convolution of two doublets. One of these is centered at δ = 0.272 mm/s, with a quadrupole splitting of *q* = 0.743 mm/s. The other one occurs at δ = 0.935 mm/s, with a quadrupole splitting of *q* = 3.184 mm/s. The intensity ratio between these two signals is 3:1, corresponding to the presence of the two different types of iron centers in this ratio (Figure 2).

The observed shifts and quadrupole splittings are in agreement with the assigned structure of **5aBF$_4$**; the signal

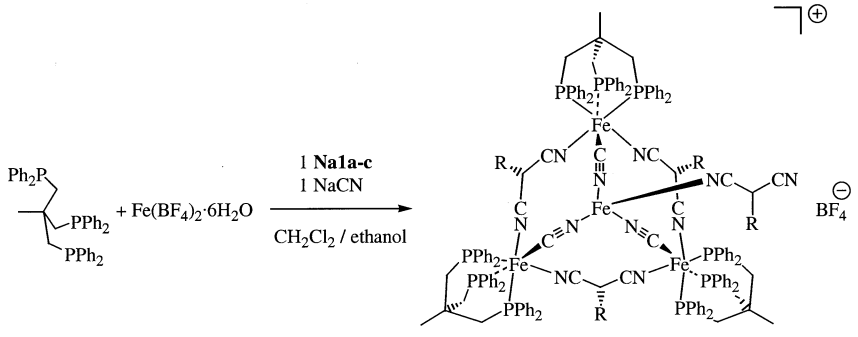

	R
5aBF$_4$	-S(O)$_2$CH$_3$
5bBF$_4$	-C(O)CH$_3$
5cBF$_4$	-C(O)OCH$_3$

Scheme 6. Synthesis of the tetranuclear compounds **5aBF$_4$**, **5bBF$_4$** and **5cBF$_4$**

Table 3. Analytical and spectroscopic data of the tetranuclear compounds **5BF$_4$** and **6BF$_4$**

No.	Formula (M [g/mol])	MS[a] m/z (%)	Magn. moment [μ_B][b][c][d]	C, H, N, P (calcd.) C, H, N, P (found)	^{57}Fe Mössbauer δ (q) [mm/s] (80 K)	IR $\tilde{\nu}$ [cm^{-1}] ν_{CN} CsI	CH_2Cl_2
5aBF$_4$	$C_{142}H_{129}BF_4Fe_4N_{11}O_8P_9S_4$	2748(4)	5.3[b]	60.16, 4.59, 5.44, 9.83	0.272 (0.743) (3 $Fe_{oct,ls}$)	2216 w; 2184 vs	2219 w; 2208 w
	(2834.9)	2123(2)	5.25[d]	59.58, 4.80, 6.02, 9.34	0.935 (3.184) (1 $Fe_{tet,hs}$)	2166 s, sh	2186 s; 2163 s
		1498(8)				2106 s	2111 m; 2105 s
5bBF$_4$	$C_{146}H_{129}BF_4Fe_4N_{11}O_4P_9$	2603(3)	4.8[c]	65.17, 4.83, 5.73	–	2218 m, 2184 vs	2205 w
	(2690.7)	1979(9)	5.2[d]	65.10, 5.25, 6.52	–		2179 s; 2166 s
		1354(10)				2105 s	2110 w, sh; 2106 m
5cBF$_4$	$C_{146}H_{129}BF_4Fe_4N_{11}O_8P_9$	2668(8)	5.2,[b] 5.5[c]	63.63, 4.72, 5.59, 10.12	–	2221 m; 2189 vs	2226 w; 2208 w
	(2754.7)	2043(8)	5.3[d]	62.96, 4.84, 5.58, 9.96	–	2172 s, sh	2191 s; 2170 s
		1418(13)				2106 s	2111 m, sh; 2107 s
5dBF$_4$	$C_{145}H_{120}BF_4Fe_4N_{16}P_9$	2589(2)	5.2[b]	65.09, 4.52, 8.38, 10.42	–	2208 m; 2165 vs	2208 w; 2164 vs
	(2675.6)	–	5.4[d]	64.43, 4.65, 8.76, 9.97	–		–
		–				2110 s	2107 s
5eBF$_4$	$C_{146}H_{117}BF_4Fe_4N_{15}O_4P_9$	2648(2)	5.3[c]	64.13, 4.31, 7.68, 10.19	–	2219 s, br	2220 w; 2194 m
	(2734.6)	–	5.5[d]	63.21, 4.53, 7.48, 10.00	–	2194 s	–
		–				2106 s	2115 s
5fBF$_4$	$C_{135}H_{117}BClF_4Fe_4N_{12}O_3P_9$	2493(4)	5.5[e]	61.85, 4.58, 6.89[e]	–	2229 w; 2213 m	–
	(2579.9)	1867(2)	5.2[d]	61.89, 4.66, 7.30	–		–
		–				2111 s	–
6BF$_4$	$C_{134}H_{117}BF_4Fe_4N_{15}P_9$	2439(15)	5.6,[b] 5.2[c]	63.70, 4.67, 8.32, 11.03	0.291 (0.788) (3 $Fe_{oct,ls}$)	2302 s; 2205 vs	–
	(2526.5)	1814(45)	5.1[d]	63.07, 4.98, 8.04, 10.82	1.006 (2.672) (1 $Fe_{tet,hs}$)	2168 vs	–
		1190(80)				2104 s	–

[a] Percentage values relate to the intensity of the signal for [*tripod*FeCN]$^+$ (m/z = 706) defined as 100 %; m/z-values are given for: M^+, [M-*tripod*]$^+$ and [M-2*tripod*]$^+$. – [b] Faraday method. – [c] Gouy method. – [d] Evans method. – [e] Elemental analysis calculated for **5fBF$_4$**·CH_3NO_2.

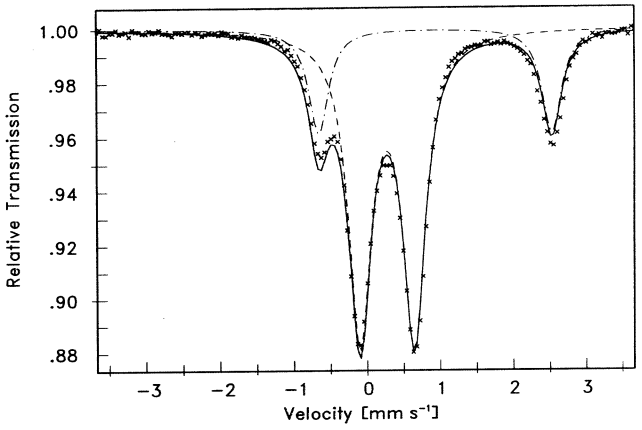

Figure 2. ^{57}Fe Mössbauer spectrum of **5aBF$_4$** (80 K)

of relative intensity 3 corresponds to three *low-spin* iron(II) units i.e. to the *tripod*iron(II) groups, each of which is coordinated to two bridging dicyanomethanide ligands and one bridging cyanide group. For comparative purposes, the Mössbauer spectrum of the tetranuclear compound [(*tripod*Fe)$_4${μ-NC−CH=CH−CN}$_6$BF$_4$](BF$_4$)$_7$,[1] which contains four *low-spin tripod*iron(II) units each coordinated to three nitrile bridging ligands, was measured. One doublet (δ = 0.363 mm/s; q = 0.255 mm/s) is observed for this compound. Shift and quadrupole splitting agree with the corresponding values of the signals assigned to *low-spin tripod*iron(II) in **5aBF$_4$**. The assignment of a *C*-coordinated μ-CN ligand to this entity, is inferred from a comparison of its Mössbauer signal with the Mössbauer data obtained for [*tripod*Fe{μ-CN}{μ-NCC(COOEt)CHC(COOEt)CN}$_2$-Fe*tripod*]BF$_4$,[21] in which one *tripod*Fe(NCR)$_2$ entity is coordinated to the carbon end of the bridging cyanide ligand and the other is coordinated to the nitrogen atom of the same ligand. One of the two observed doublets corresponds almost exactly to the doublet observed for [(*tripod*Fe)$_4${μ-NC−CH=CH−CN}$_6$BF$_4$](BF$_4$)$_7$ with three *N*-coordinated nitrile ligands; the other is characterized by the parameters (δ = 0.341 mm/s; q = 0.688 mm/s), which are very similar to those characterizing the Mössbauer data of the *tripod*iron(II) entity in **5aBF$_4$**. This is taken as a strong indication for the *C*-coordination of the cyano groups to the *tripod*iron(II) entities in **5aBF$_4$**. The magnetic moment observed for **5aBF$_4$** (μ = 5.3 μ_B, Table 3) corresponds closely to the *spin-only* value ($\mu_{s.o.}$ = 4.9 μ_B) for a tetrahedral *high-spin* iron(II) center. The Mössbauer data for this type of iron compound are in a range [$(FeCl_4)^{2-}$: δ = 1.0 mm/s; q = 2.55 mm/s[22−24]] which indicates that the apical iron(II) center with its three *N*-coordinated cyano ligands and one terminal nitrile ligand has a *high-spin* electron configuration.

The same type of reaction, as has been explicitly described for **Na1a** leading to **5aBF$_4$**, occurs if **Na1b** and **Na1c** are used as the dinitrile components, hence leading to **5bBF$_4$** and **5cBF$_4$** respectively (Scheme 6). The spectroscopic and magnetic properties of **5bBF$_4$** and **5cBF$_4$** (Table 3) are very similar to those discussed in detail for **5aBF$_4$**. Microanalyses are also in agreement with the formulae given (Table 3).

A definite proof of the structure of compounds $\mathbf{5BF_4}$ comes from the X-ray analysis of $\mathbf{5aBF_4}$. Suitable single crystals of $\mathbf{5aBF_4}\cdot 1.5\ CH_3NO_2\cdot 2.2\ C_4H_8O_2$ could be grown from nitromethane solutions of $\mathbf{5aBF_4}$, by slow vapor phase diffusion of ethyl acetate at room temperature (Figure 3).

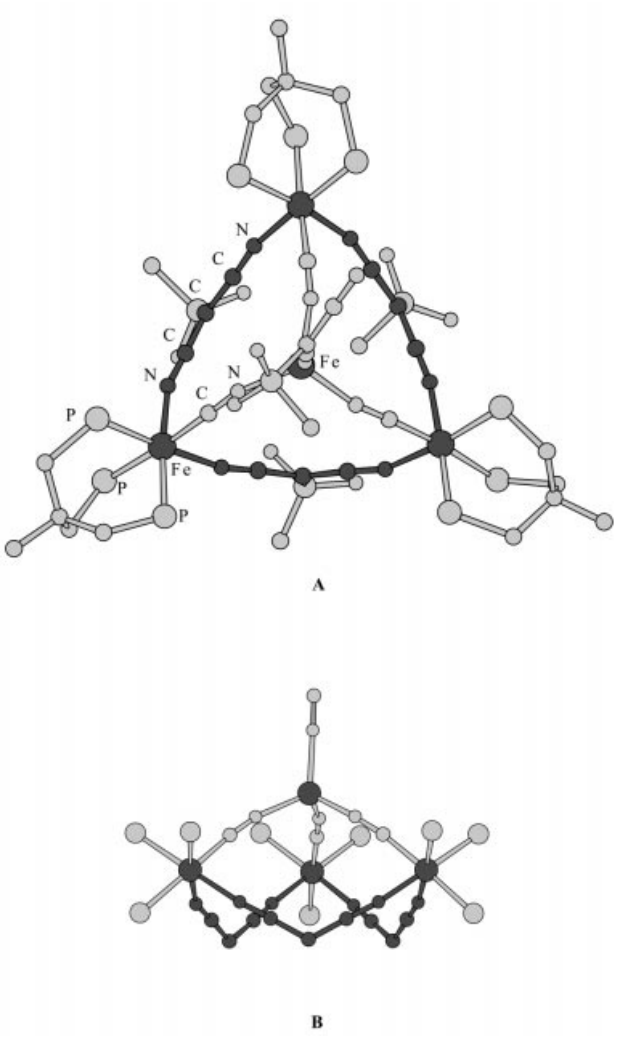

Figure 3. Two views of the cation $\mathbf{5a^+}$; for the sake of clarity only part of the ligand periphery is shown; Fe_{oct}= octahedrally coordinated iron(II); Fe_{tet}= tetrahedrally coordinated iron(II); selected bond lengths [pm] and angles [°]: $Fe_{oct}-P_{\mathit{cis}CN}$ 224.9(2) to 226.7(2), $Fe_{oct}-P_{\mathit{trans}CN}$ 231.7(2) to 232.6(2), $Fe_{oct}-N$ 196.0(7) to 200.5(7), $Fe_{oct}-C_{CN}$ 191(1) to 193(1), $Fe_{tet}-N_{CN}$ 199.2(6) to 201.1(7), $Fe_{tet}-N$ 204.3(7), $C_{CN}-N_{CN}$ 115(1) to 118(1), C−N 113(1) to 117(1), $C-C_{CN}$ 139(1) to 144(1); P−Fe−P 85.1(1) to 91.3(1), P−Fe−C 91.8(3) to 94.0(3), 174.4(3) to 177.6(3), P−Fe−N 90.1(3) to 98.2(3), $N-Fe_{oct}-N$ 83.8(3) to 84.7(3), $N_{CN}-Fe_{tet}-N_{CN}$ 104.1(2) to 107.6(2), $N_{CN}-Fe_{tet}-N$ 110.0(3) to 116.1(3), $Fe_{oct}-C_{CN}-N_{CN}$ 173(1) to 175(1), $Fe_{tet}-N_{CN}-C_{CN}$ 165(1) to 167(1)

The cation $\mathbf{5a^+}$ consists of a triangle spanned by three *tripod*iron(II) units, which are linked by three bridging (methylsulfonyl)dicyanomethanide ligands (Figure 3 **A**). Five coordination sites of the octahedrally coordinated *tripod*iron(II) centers (Fe_{oct}) are thus used to form the bonds within this triangle and to the *tripod* ligands. In each case the sixth position is occupied by a *C*-bonded cyano ligand. The N-termini of these three cyano ligands coordinate to the apical iron center, which has a tetrahedral coordination (Fe_{tet}), with the fourth position being occupied by a terminal (methylsulfonyl)dicyanomethanide ligand, which is coordinated by one nitrile functionality (Figure 3 **A**). The angles around Fe_{oct} are close to the ideal values of a coordination octahedron, although individual deviations of up to 8° (Figure 3) indicate some strain within the cage as a whole. The assumption that the μ-CN groups are *C*-bonded to the *tripod*iron(II) entities, which had been inferred from Mössbauer analysis, is corroborated by the observation that with this assignment of atom types to the bridging cyano groups, reasonable temperature factors are obtained for both carbon and nitrogen during such a refinement. Another argument in favor of this hypothesis comes from the observation that the Fe−P distances involving phosphorus atoms *trans* to the cyano ligands are some 6 pm longer than the remaining Fe−P distances, which involve phosphorus atoms which are *trans* to the organic nitrile groups (Figure 3). In addition, the Fe−C bonds are distinctly shorter than the Fe−N bonds for all three basal iron centers. The $Fe_{oct}-C_{CN}-N_{CN}$-groups are only slightly bent, while the angles $Fe_{tet}-N_{CN}-C_{CN}$ deviate from 180° to a larger extent (Figure 3). The distances $Fe_{tet}-N_{CN}$ are around 200 pm. The $Fe_{tet}-N$ distance to the terminal ligand is 204 pm. The $Fe_{tet}-N$ bonds, radiating from the tetrahedrally coordinated apical *high-spin* iron center, are definitely longer than those involving the basal, octahedrally coordinated, *low-spin* iron centers. The observed $Fe_{tet}-N$ distances (Figure 3) are in agreement with the observed values for other tetrahedrally coordinated *high-spin* iron(II) species.[25] When $\mathbf{1e^-}$ and $\mathbf{1f^-}$ are used as the dicyanomethanide components in the synthesis of $\mathbf{5BF_4}$, the reaction proceeds in a similar way (Scheme 7).

The resulting compounds $\mathbf{5eBF_4}$ and $\mathbf{5fBF_4}$ are less soluble than $\mathbf{5aBF_4}$, $\mathbf{5bBF_4}$ and $\mathbf{5cBF_4}$. They are obtained as red precipitates from the reaction solutions. These precipitates are dissolved in nitromethane for purification. After filtration through silica gel, pure samples of $\mathbf{5eBF_4}$ and $\mathbf{5fBF_4}$ are obtained from these solutions by crystallization. Cubic crystals are obtained by vapor phase diffusion of diethyl ether into nitromethane solutions of $\mathbf{5eBF_4}$ and $\mathbf{5fBF_4}$. Both compounds crystallize in the cubic space group $P\bar{4}3n$. In both cases the structures are strongly affected by disorder problems. There are positions within the crystals that are occupied by solvent molecules with varying degrees of disorder. There is also disorder with respect to the apical ligand of the tetrahedrally coordinated iron center, which is confined by crystallographic symmetry to lie on a crystallographic C_3 axis. This disorder cannot be completely resolved, neither for $\mathbf{5eBF_4}$, nor for $\mathbf{5fBF_4}$. The best solution for $\mathbf{5e^+}$ is obtained by assigning a fluoride ligand to this position. For $\mathbf{5f^+}$ a chloride ligand gives the most satisfactory result. The overall geometry of the framework of the tetrahedral cage in $\mathbf{5e^+}$, including the *tripod* ligands, is determined by structure analysis without any doubt. The only problem with regard to assigning individual atoms to the otherwise well-defined positions, remains for the μ-CN groups. The best solution is obtained if the CN groups are

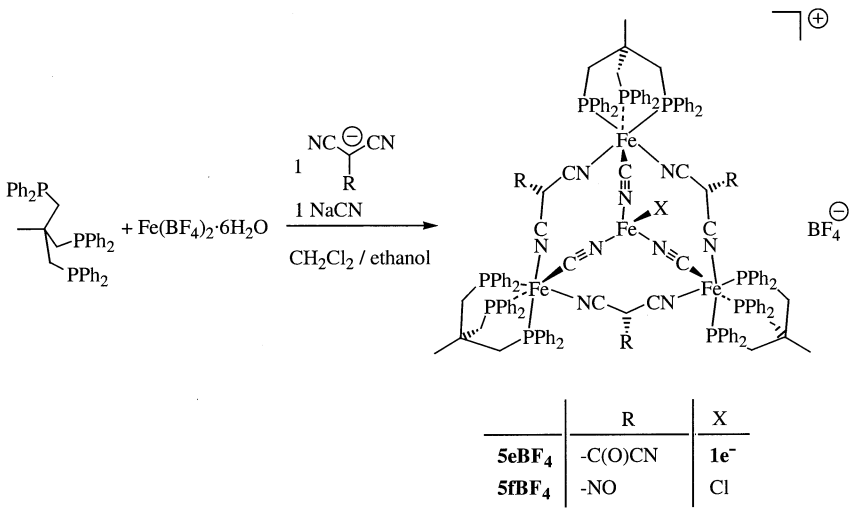

	R	X
5eBF$_4$	-C(O)CN	**1e$^-$**
5fBF$_4$	-NO	Cl

Scheme 7. Synthesis of the tetranuclear compounds **5eBF$_4$** and **5fBF$_4$**

oriented as described for **5a**$^+$. For **5f** $^+$ the overall cage structure is similarly well defined. Here however, the C(NO) linkers joining the coordinated nitrile groups of the bridging dicyanomethanide ligands show disorder, indicating that the symmetry of the η^2-coordination of this ligand does not conform exactly to the crystallographically imposed C_3 symmetry. In view of their inaccuracy in quantitative detail and their close similarity in the overall structure of the cage and the coordination environments, individual data are not discussed here. However, the structural data have been deposited. It appears that the fact that **5aBF$_4$** contains a large C_s-symmetric organic ligand in the apical position is responsible for effectively breaking the *pseudo* symmetry of the crystals. As a result, its structure could be solved without major interference by disorder problems, the only compound in the series of compounds **5BF$_4$**. The lower crystal symmetry of **5aBF$_4$** ($P2_1/n$) as compared with **5eBF$_4$** and **5fBF$_4$** (and also with **5dBF$_4$**, see below) is already macroscopically apparent by looking at the shape of the crystals. The crystals of **5aBF$_4$** form parallelepipeds, whilst those of the others form cubes or hexagonal plates.

A problem associated with compounds **5BF$_4$** is that they undergo easy exchange of their apical ligand. Thus, structure analysis showed that in the crystal specimen analyzed, **5e**$^+$ has an apical ligand with the diffraction power of a fluoride or a hydroxy group. It definitely shows that the molecule in the crystal does not contain a ligand such as **1e**$^-$ or a chloride ion in the apical position. On the other hand, FAB$^+$ mass spectrometry (Table 3) of the bulk crystalline material clarifies that the parent molecular ions observed in the gas phase do not contain either F^- or OH^-. Three types of parent ions are observed, together with their daughter ion $[(tripod\text{Fe})_3\{\mu\text{-NC}-\text{C[C(O)CN]}-\text{CN}\}_3\{\mu\text{-CN}\}_3\text{Fe}]^+$ (m/z = 2530). The mass differences between these three types of parent ions and the daughter ions are 35, 118 and 166, respectively. These mass differences are interpreted as being due to the loss of three different types of apical ligands; chloride, tricyanoethenolate (**1e**$^-$) and pentacyanopropenide ($C_8N_5^-$). Elemental analysis of the bulk material of **5eBF$_4$** shows that **1e**$^-$ is the apical ligand in the original sample (Table 3). It appears that the different processes of handling the probes during FAB$^+$ mass spectrometry, as well as during crystal growth, causes the exchange of the apical ligand. The fluoride ion (crystal structure) may have been incorporated whilst **5eBF$_4$** was in solution for several days which is necessary in order to obtain crystals. The only explanation for the observed incorporation of the chloride ion is an exchange during the processing steps where dichloromethane was used as a solvent. The presence of a pentacyanopropenide ion as an apical ligand, which is seen by mass spectrometry, can be explained by the tendency of polycyano-substituted C_2 entities to form this anion under various conditions.[15] Small peaks attributed to the exchange of the apical ligand by pentacyanopropenide are also observed for **5aBF$_4$**, **5cBF$_4$** and **5fBF$_4$**. The peak corresponding to the molecular ion **5e**$^+$ has a lower intensity than the peaks observed for the chloride and pentacyanopropenide derivative. These two latter molecular ions show daughter ions at m/z = 1940 and 2071, respectively, which correspond to the loss of one *tripod* ligand. This is consistent with the observation that **5a**, **5b**$^+$ and **5c**$^+$, as well as **6**$^+$, show prominent peaks which can be attributed to the loss of one or two *tripod* ligands from their parent ions (Table 3). The mass spectrum of **5fBF$_4$** shows a strong signal for the parent ion with the chloride ion as the apical ligand. This is consistent with the result from the X-ray analysis of **5fBF$_4$**. In addition, the mass spectrum of **5fBF$_4$** shows a molecular ion which corresponds to the exchange of the apical chloride ligand by **1f**$^-$ [m/z (%) = 2552 (8)], and a peak which corresponds to the exchange by pentacyanopropenide [m/z (%) = 2624 (3)]. The ease of exchange of the apical ligands as observed in the mass-spectrometric analyses, and the tendency to include solvent molecules as seen by the X-ray analyses, is mirrored by the microanalytical data (Table 3), which are, in some cases, not as accurate as could be expected. The magnetic moments

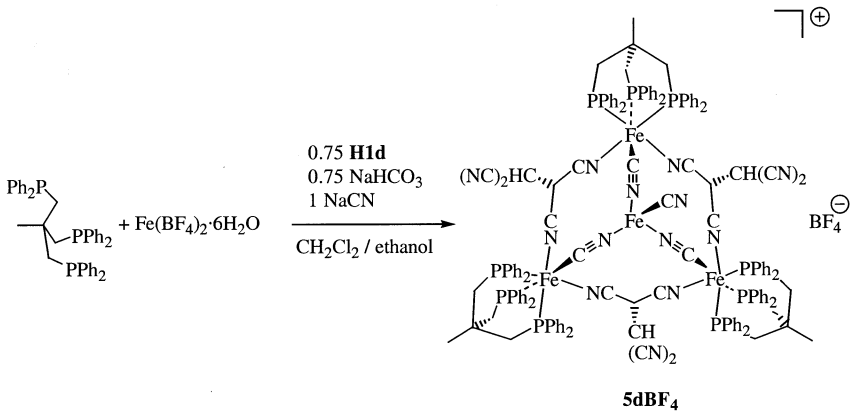

Scheme 8. Synthesis of the tetranuclear compound **5dBF$_4$** according to method **A**

of **5eBF$_4$** and **5fBF$_4$** are around the value of $\mu_{s.o.} = 4.9\ \mu_B$, as expected for a *high-spin* tetrahedral d^6 species (Table 3). It is known that with iron(II) as the d^6 center, spin−orbit coupling tends to result in moments slightly higher than the *spin-only* values.[26] The IR data of **5eBF$_4$** and **5fBF$_4$** (Table 3) are in agreement with the formulae given; the ν_{CN} bands compare well with the ones discussed for **5aBF$_4$**, **5bBF$_4$** and **5cBF$_4$**.

The reaction of $Fe^{II}aq(BF_4)_2$ and *tripod* in dichloromethane/ethanol (1:1) with 1,1,2,2-tetracyanoethane, **H1d**, produces **5dBF$_4$** on addition of stoichiometric amounts of sodium cyanide and sodium bicarbonate (method **A**) (Scheme 8). The initial pale yellow color of the $Fe^{II}aq(BF_4)_2$/*tripod* mixture immediately turns red on addition of **H1d**. No further color change is observed when sodium cyanide and sodium bicarbonate are added to the solution. However, over a period of 10 h the color of the solution changes to black, while an orange-brown precipitate forms. This precipitate is dissolved in nitromethane and purified by filtration and crystallization from nitromethane/dichloromethane/diethyl ether giving **5dBF$_4$** (40%).

An alternative synthesis of **5dBF$_4$** consists of heating **3dBF$_4$** to reflux in dichloromethane/ethanol (1:1) for 10 h (method **B**) (Scheme 9). The initial red color (**3dBF$_4$**) gradually changes to a dark red-brown. Purification by chromatography and crystallization yields **5dBF$_4$** (40%).

Yet another procedure for the synthesis of **5d$^+$** consists of the reaction of a mixture of *tripod* and $FeCl_2$ in dichloromethane/ethanol (1:1) with NaTCNE [27,28] (method **C**) (Scheme 10). On addition of NaTCNE, the solution becomes very dark which is characteristic of solutions of NaTCNE. Over a period of 10 h at room temperature, an orange-red precipitate forms, which is purified by crystallization giving **5dPF$_6$** (55%).

The cyanide ligands in **5d$^+$** must result from a partial disintegration of the TCNE-type precursors in the last two procedures **B** and **C**.

Crystals of **5dBF$_4$** have been obtained from batches produced in routes **B** and **C**. In an independent method, principally according to method **C** but by adding tetrafluoroborate as the counterion, another batch was produced from which crystals could also be obtained. The problem encountered with the structure analyses of these three different types of crystals is very similar to the one already discussed with regard to the structure analyses of **5eBF$_4$** and **5fBF$_4$**. All three types of crystals belong to highly symmetric space groups ($P\bar{4}3n$ and $P31c$), that impose crystallographic trigonal symmetry onto the tetranuclear cations. This symmetry does not correspond to the true molecular symmetry, since the $C(CN)_2H$ groups show disorder around their $C-C(CN)_2H$ bond. In addition, as already observed for **5eBF$_4$** and **5fBF$_4$**, the apical ligands of the tetrahedrally co-

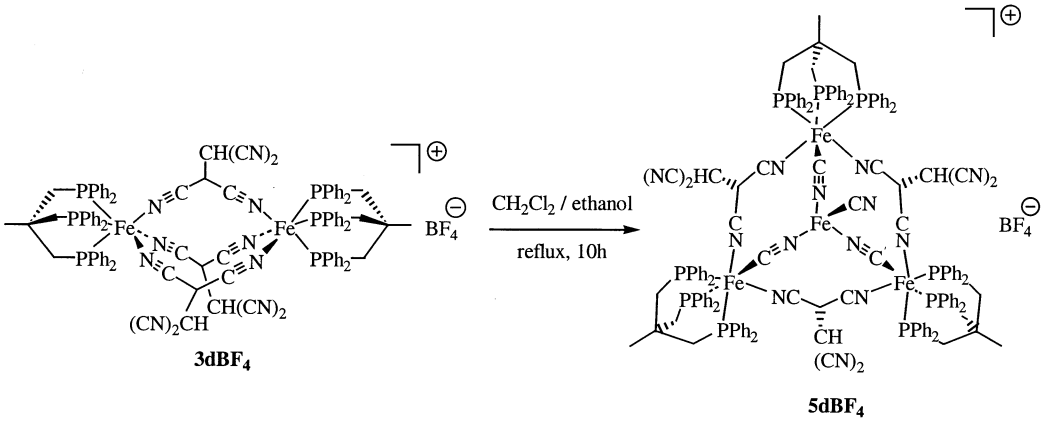

Scheme 9. Synthesis of the tetranuclear compound **5dBF$_4$** according to method **B**

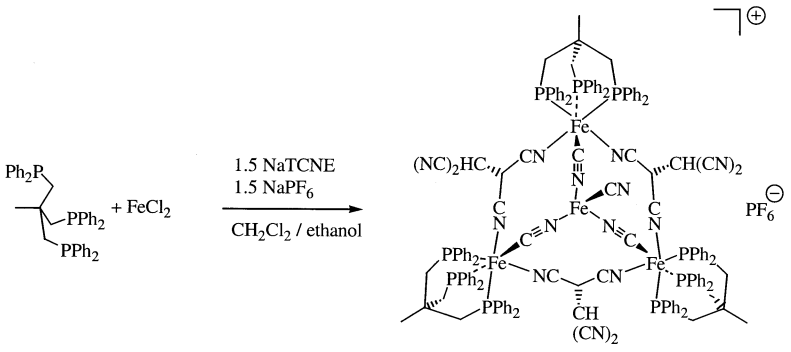

5dPF$_6$

Scheme 10. Synthesis of the tetranuclear compound **5dPF$_6$** according to method **C**

ordinated iron centers can be easily exchanged. In the crystals obtained by method **C** with hexafluorophosphate as the counterion, a chloride ion is in the apical position. The crystals produced by the same method, but with tetrafluoroborate as the counterion, are found to have cyanide as the apical ligand. In these crystals, there is not only rotational disorder of the $C(CN)_2H$ groups, but also a strong indication for the presence of $C(CN)H_2$ groups instead of $C(CN)_2H$ entities. With this assignment, the structure can be refined to an agreement factor of $R_1 = 8.7\%$ (Table 7). The quality of the individual geometric parameters is nevertheless low, due to the many disordered solvent molecules involved. The crystals produced according to method **B** are found to contain F^- or OH^- as the apical ligand. The organic bridging groups show the same type of disorder as discussed above, with the best solution being obtained by describing the rotationally disordered substituent as the $C(CN)H_2$ group. While all these structure analyses unequivocally prove the persistence of a [(*tripod*Fe)$_3${μ-NC−C(R)−CN}$_3${μ-CN}$_3$Fe−X] core, they cannot definitely elucidate the nature of R and X. FAB^+ mass spectra are more conclusive with regard to the nature of R in the bulk materials. The molecular ions are consistent with R = $C(CN)_2H$. Satellite peaks are found for R = $C(CN)H_2$. This indicates that the bulk material contains R = $C(CN)_2H$, as well as R = $C(CN)H_2$ as the substituent at the $RC(CN)_2$ bridging unit. Mass spectra are less conclusive with respect to the nature of the apical ligand X. In all spectra there is a prominent peak for the parent ion with X = CN^-. However, there are peaks for X = F^-/OH^-, Cl^-, CNO^- and $C_8N_5^-$ as well. The situation is thus very similar to the one described for **5eBF$_4$** and **5fBF$_4$**, and the final answer must be obtained from elemental analysis. Considering all combinations of possible constituents, the most satisfactory agreement is X = CN^- (Table 3). The magnetic moment of **5dBF$_4$** is in the range observed for the other compounds **5BF$_4$** (Table 3). The bridging cyano ligands are evident from their IR absorptions, as are the $RC(CN)_2$ building blocks (Table 3).

The reaction of $Fe^{II}aq(BF_4)_2$ and *tripod* in dichloromethane/ethanol (1:1) with sodium dicyanamide, **Na2**, and sodium cyanide gives **6BF$_4$** in a procedure very similar to the one used for the preparation of compounds **5BF$_4$** (Scheme 11). **6BF$_4$** is obtained as a red precipitate, which is purified by crystallization giving a red crystalline material. Although none of the many analyzed crystals gave good diffraction patterns so as to allow X-ray analysis, the spectroscopic and analytical data (Table 3) clearly prove that **6**$^+$ has a framework analogous to the one which characterizes the series of cations **5**$^+$. The magnetic moment and the infrared data (Table 3) support the above statement. The IR spectra show ν_{CN} bands that are characteristic of the dicyanamide ligand and the Fe(μ-NC)$_3$ group. The FAB^+ mass spectrum shows prominent peaks for the molecular

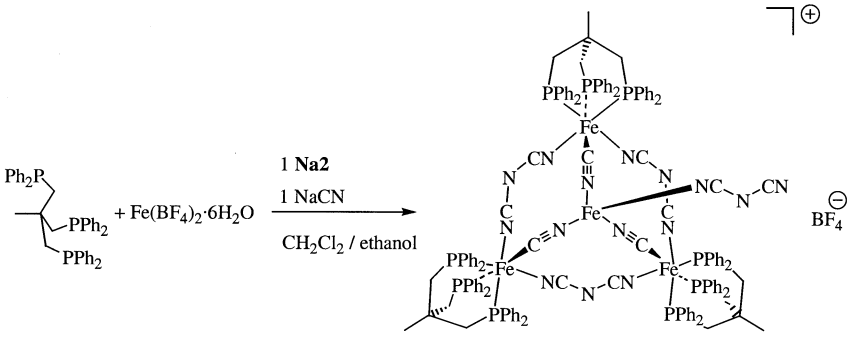

6BF$_4$

Scheme 11. Synthesis of the tetranuclear compound **6BF$_4$**

Table 4. UV/Vis and cyclic voltammetric data of compounds **3BF$_4$**, **4BF$_4$**, **5BF$_4$** and **6BF$_4$**

No.	UV (CH_2Cl_2)		CV (CH_2Cl_2, SCE)			No.	UV (CH_2Cl_2)		CV (CH_2Cl_2, SCE)	
	λ [cm^{-1}]	(ε [$M^{-1}cm^{-1}$])	$E_{1/2}$ [mV]	(ΔE)	K_C [a]		λ [cm^{-1}]	(ε [$M^{-1}cm^{-1}$])	$E_{1/2}$ [mV]	(ΔE)
3aBF$_4$	19600	(1900)	1120	(110)	$10^{4.7}$	**5aBF$_4$**	19800	(800)	1045	(110)
	24300	(1100)	1400	(116)			23000	(2200)		
							27900 sh	(6300)		
3bBF$_4$	19700	(2300)	1058	(105)	$10^{4.6}$	**5bBF$_4$**	19600	(1200)	990	(155)
	24500	(1000)	1328	(115)			22400	(2600)		
							27700 sh	(8300)		
3cBF$_4$	19700	(2100)	1000	(120)	$10^{5.4}$	**5cBF$_4$**	19600	(1300)	948	(115)
	24400	(800)	1320	(115)			22800	(2900)		
							27700 sh	(10000)		
3dBF$_4$	19500	(2200)	1020	(101)	–	**5dBF$_4$**	19400	(1500)	1000	(130)
	23900	(1300)					23000	(3500)		
							27000 sh	(9500)		
						5eBF$_4$	19800	(2100)	873	(150)
							22400	(2800)		
							27800 sh	(11000)		
						5fBF$_4$	19600	(3000)	1140	(80)
							22600	(7500)	(CH_3CN)	
							28400 sh	(16000)		
4BF$_4$	19100	(2100)	910	(113)	$10^{4.4}$	**6BF$_4$**	19500	(1800)	886	(112)
	24200	(900)	1150	(108)			22200	(2200)	1120	(140)
							28500 sh	(6200)		

[a] Equilibrium constants K_C of the comproportionation reaction (Scheme 12) calculated by: $K_C = \exp(\Delta E_{1/2}/25.69)$; $\Delta E_{1/2}$ in mV.

ion **6**$^+$ and for the daughter ions derived from the consecutive loss of two *tripod* ligands. The Mössbauer spectrum of **6BF$_4$** shows a signature which is very similar to the one observed for **5aBF$_4$** (Table 3). It demonstrates the presence of *high-spin* iron(II) and *low-spin* iron(II) in a ratio of 1:3. The microanalytical data are in full accord with the assigned formula.

Electrochemistry and UV/Vis Spectra

All compounds **3BF$_4$** to **6BF$_4$** undergo at least one one-electron oxidation. For the binuclear compounds **3BF$_4$**, the corresponding potentials are between $E_{1/2}$ = 910 mV (**4BF$_4$**) and 1120 mV (**3aBF$_4$**) (Table 4).

A second one-electron oxidation step is observed between $E_{1/2}$ = 1150 mV (**4BF$_4$**) and 1400 mV (**3aBF$_4$**) (Table 4). This second step is reversible for all binuclear compounds except **3dBF$_4$**, for which an irreversible electron transfer at E_{pa} = 1430 mV is observed. The observation of two distinctly different one-electron oxidation steps demonstrates that the iron centers take notice of each other. The distance between the two iron centers is around 700 pm (Figure 1) and the iron centers are joined by five-atom linkers. Both these facts are in favor of the stability of a mixed-valence Fe^{II}/Fe^{III} species. The equilibrium constant K_C for the comproportionation reaction (Scheme 12), as deduced from the oxidation potentials, is in fact rather high throughout (Table 4).[29] With a value of around 10^5, it characterizes the Fe^{II}/Fe^{III} complexes as class III mixed-valent species.[30]

$$M\sim\sim M + M^{ox}\sim\sim M^{ox} \underset{}{\overset{K_C}{\rightleftharpoons}} 2\ M\sim\sim M^{ox}$$

Scheme 12. Comproportionation equilibrium for mixed-valent dinuclear complexes

This means, that the iron centers and the ligands form a conjugated system together.[31,32]

The tetranuclear compounds **5BF$_4$** show only one reversible one-electron oxidation. A second reversible oxidation is observed for **6BF$_4$**, with its dicyanamide ligands (Table 4). Within each pair of compounds **3BF$_4$** and **5BF$_4$** (**4BF$_4$** and **6BF$_4$**), the first one-electron oxidation step occurs at similar potentials (Table 4), with a tendency of compounds **5BF$_4$** to be somewhat easier to oxidize than the corresponding compounds **3BF$_4$**. The similarity of the oxidation potentials of **3BF$_4$** and **5BF$_4$** shows that the oxidation of **5BF$_4$** is not centered at its *high-spin* iron(II) center.

The UV/Vis spectra of the different compounds **3BF$_4$** are rather similar (Figure 4). Bands occur at $\lambda \approx$ 19500 and 24000 cm^{-1} (Figure 4, Table 4). A similar pattern is observed for [*tripod*$Fe^{II}(NCMe)_3]^{2+}$ [33] (λ = 20500 and 26000 cm^{-1}), which has three organonitrile groups coordinated to a *tripod*iron(II) entity and is a *low-spin* compound, as are compounds **3BF$_4$**. Therefore, it is assumed that the bands observed for **3BF$_4$** correspond to the spectral signature of *low-spin tripod*$Fe^{II}(NCR)_3$ entities. Within the series of compounds **3BF$_4$** there is a slight shift of the relevant absorption energies (Table 4).

Compounds **5BF$_4$** and **6BF$_4$** show similar absorption patterns through their whole series. The bands at $\lambda \approx$ 19500 and 23000 cm^{-1} (Figure 4, Table 4) are typical for *low-spin tripod*$Fe^{II}L_3$ compounds. In the case of **5BF$_4$** and **6BF$_4$**, two of these ligands are nitrile groups from the organic bridging ligand, the third ligand is a cyano group acting as a bridging ligand to bind a tetrahedral *high-spin* iron(II) center. There is no indication in the spectra of **5BF$_4$** and **6BF$_4$** of any significant contribution from this *high-spin*

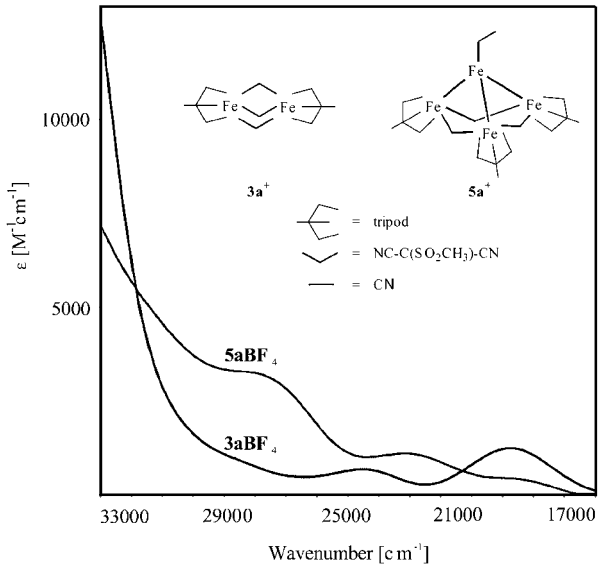

Figure 4. UV/Vis spectra of **3aBF$_4$** and **5aBF$_4$**

iron(II) center occurring in the long-wavelength range of the spectra (Figure 4, Table 4).

Conclusion

The *tripod* ligands, $Fe^{II}aq(BF_4)_2$ and dinitrile constituents engage in a self-assembly process to produce binuclear $[tripodFe\{\mu\text{-}NC-C(R)-CN\}_3Fetripod]^+$ or − in the presence of cyanide − tetranuclear compounds $[(tripodFe)_3\{\mu\text{-}NC-C(R)-CN\}_3\{\mu\text{-}CN\}_3Fe-X]^+$, exclusively. The self-organization process, which exclusively leads to $[tripodFe\{\mu\text{-}NC-C(R)-CN\}_3Fetripod]^+$ with the angular clamp-type ligands $[NC-C(R)-CN]^-$, may be switched to the exclusive formation of tetrahedral aggregates $[(tripodFe)_3\{\mu\text{-}NC-C(R)-CN\}_3\{\mu\text{-}CN\}_3Fe-X]^+$ by the interference of the linear rod-type ligand cyanide. The tetranuclear compounds $[(tripodFe)_3\{\mu\text{-}NC-C(R)-CN\}_3\{\mu\text{-}CN\}_3Fe-X]^+$ contain three *low-spin* $tripodFe^{II}L_3$ units and one tetrahedral *high-spin* iron(II) entity in one supramolecular aggregate.

The electrochemistry shows that compounds $[tripodFe\{\mu\text{-}NC-C(R)-CN\}_3Fetripod]^+$ form mixed-valent Fe^{II}/Fe^{III}-species of type III. They are stable against disproportionation into Fe^{II}/Fe^{II}- and Fe^{III}/Fe^{III}-species.

Experimental Section

General: All manipulations were carried out under argon by means of standard Schlenk techniques. All solvents were dried by standard methods [34] and distilled under argon. Silica gel and Kieselgur, used for filtration operations and chromatography, were degassed at 1 mbar for 24 h and saturated with argon. The compounds *tripod*,[35,36] $Fe(BF_4)_2{\cdot}6H_2O$,[37] (methylsulfonyl)malononitrile hydrochloride,[9] 1,1,2,2-tetracyanoethane,[14] NaTCNE,[27] tetramethylammonium tricyanethenolate[15] and sodium nitrosodicyanmethanide[16] were prepared in accordance to, or by adaptation of, literature procedures. All other chemicals were obtained from commercial suppliers and used without further purification. − NMR: Bruker Avance DPX200 spectrometer at 200.13 MHz (^{1}H), 50.323 MHz (^{13}C), 81.014 MHz (^{31}P); T = 303 K; chemical shifts (δ) in ppm with respect to CD_2Cl_2 (^{1}H: δ = 5.32; ^{13}C: δ = 53.5), [D$_6$]acetone (^{1}H: δ = 2.05; ^{13}C: δ = 20.8, 206.1) or [D$_6$]DMSO, (^{1}H: δ = 2.50; ^{13}C: δ = 39.4) as internal standards; ^{31}P chemical shifts (δ) in ppm with respect to 85% H_3PO_4 (^{31}P: δ = 0) as external standard; CD_2Cl_2, [D$_6$]acetone and [D$_6$]DMSO used, for NMR-spectroscopic measurements, were degassed by three successive "freeze-pump-thaw" cycles and dried over 4-Å molecular sieves. − Magnetic measurements: Faraday method: electromagnet B-E 1 C-8 and controller unit B-H 15 (Bruker); M 25 D-S balance (Sartorius). Gouy method: Sherwood Scientific Magnetic Susceptibility Balance (Johnson & Matthey). Evans method: Bruker Avance DPX200 spectrometer at 200.13 MHz (^{1}H); solvent: CD_2Cl_2; standard: DPPH (diphenylpikrylhydrazyl); T = 303 K. − IR: Biorad Excalibur spectralphotometer FTS 3000 [CsI discs or solutions (CaF_2 windows)]. − UV/Vis spectra: Perkin−Elmer UV/Vis spectralphotometer Lambda 9; ca.10^{-3} M solutions in CH_2Cl_2. − MS: Finnigan MAT 8320, VG ZAB 2F; FAB (Xenon; matrix: 4-nitrobenzyl alcohol). − Cyclic voltammetry: EG&G Princeton Applied Research model 273; potentials in mV versus SCE at a glassy carbon electrode at 25 °C; solutions of compounds: ca.10^{-3} M in 0.1 M Bu_4NPF_6 in CH_3CN or CH_2Cl_2. − Elemental analyses: Microanalytical Laboratory of the Organisch-Chemisches Institut, Universität Heidelberg.

Preparation of the Compounds

Na[NCC(R)CN] [Na1: R = SO_2CH_3 (Na1a), $COCH_3$ (Na1b), CO_2CH_3 (Na1c)]:[10,12,13] **Na1a** was synthesized from the hydrochloride of (methylsulfonyl)malononitrile (279 mg; 1.54 mmol) by reaction with a slight excess of sodium bicarbonate (267 mg; 3.18 mmol) in water.[9] After drying the reaction mixture and filtering with 5 mL acetone, the product was isolated by precipitation with excess diethyl ether. 187 mg (73%) of a white solid was obtained after isolation and drying in vacuo. − $C_4H_3N_2NaO_2S$ (166.1): calcd. C 28.92, H 1.82, N 16.86; found C 29.23, H 2.56, N 16.88. − ^{1}H NMR ([D$_6$]acetone): δ = 2.88 (s). − ^{13}C NMR ([D$_6$]DMSO): δ = 42.2 (s, NC*C*CN), 46.3 (s, CH_3), 120.4 (s, CN). − IR (CsI): $\tilde{\nu}$ = 2187 m, 2160 s (CN); 1295 vs, 1137 vs (SO_2) cm^{-1}. − **Na1b** was prepared by dropwise addition of acetyl chloride (5.3 g; 68 mmol) to an ice-cooled solution of malononitrile (4.5 g; 68 mmol) in 10 mL of THF and sodium hydroxide (5.2 g; 130 mmol) in 10 mL of water. A light brown suspension formed, which was filtered after warming to room temperature. The precipitate was washed twice with 2 mL of ice-cold water, dried in vacuo and recrystallized from ethyl acetate/ethanol (20:1; 100 mL) yielding 6.4 g (65%) of a white powder. For elemental analysis the product was recrystallized from acetone/diethyl ether and dried in vacuo. − $C_5H_3N_2NaO$ (130.1): calcd. C 46.17, H 2.32, N 21.54; found C 46.25, H 2.52, N 21.36. − ^{1}H NMR ([D$_6$]DMSO): δ = 1.86 (s). − ^{13}C NMR ([D$_6$]DMSO): δ = 26.4 (s, CH_3); 47.9 (s, NC*C*CN); 121.8 (s, CN); 123.9 (s, CN); 191.0 (s, CO). − **IR** (CsI): $\tilde{\nu}$ = 2219 vs, 2193 vs, 2184 s,sh (CN); 1572 vs. (CO) cm^{-1}.− **Na1c** was prepared by dropwise addition of a mixture of methyl chloroformate (7.8 g; 82 mmol) and malononitrile (5.1 g; 77 mmol) in 10 mL of THF, to an ice-cooled solution of sodium hydroxide (6.2 g; 154 mmol) in 15 mL of water. A white suspension formed, which was filtered after warming to room temperature. The white precipitate was washed twice with 3 mL of ice-cold water, dried in vacuo and recrystallized from ethyl acetate (100 mL) yielding 6.0 g (48%) of light yellow needle-type crystals. − $C_5H_3N_2NaO_2$ (146.1): calcd.

C 41.11, H 2.07, N 19.18; found C 41.08, H 2.34, N 19.07. − ^{1}H NMR ([D$_6$]acetone): δ = 3.51 (s). − ^{13}C NMR ([D$_6$]acetone): δ = 32.3 (s, NC*C*CN); 51.0 (s, CH_3); 122.0 (s, CN); 123.1 (s, CN); 172.7 (s, COO). − IR (CsI): $\tilde{\nu}$ = 2216 vs, 2184 s (CN); 1648 vs, br (CO) cm^{-1}.

[(*tripod*Fe)$_2${μ-NCC(R)CN}$_3$]BF$_4$ [3BF$_4$: R = SO_2CH_3 (3aBF$_4$), $COCH_3$ (3bBF$_4$), CO_2CH_3 (3cBF$_4$)] and [(*tripod*Fe)$_2${μ-NCNCN}$_3$]BF$_4$ (4BF$_4$): Na1a, **Na1a**, **Na1c** or **Na2** (1.5 mmol) was added as a solid, in one portion, to a solution of Fe^{II}aq(BF$_4$)$_2$ (338 mg, 1 mmol) and *tripod* (625 mg, 1 mmol) in acetone. An immediate color change from pale yellow to red was observed. After stirring for 1 h at room temperature, the solvent was evaporated. The red residue was washed once with diethyl ether and dried in vacuo. Filtration with dichloromethane through 1 cm of Kieselgur and concentration of the red filtrate yielded the products as red to violet microcrystalline solids. For purification, the products were recrystallized. Yields and solvents of crystallization: **3aBF$_4$** [74% (acetone/diethyl ether)], **3bBF$_4$** [70% (dichloromethane/ethanol)], **3cBF$_4$** [78% (acetone/diethyl ether)], **4BF$_4$** [59% (dichloromethane/ethanol)]. For further analytical and spectroscopic data of the compounds see Tables 1, 2 and 4.

[(*tripod*Fe)$_2${μ-NCC[CH(CN)$_2$]CN}$_3$]BF$_4$ (3dBF$_4$): Solid **H1d** (1.5 mmol) was added in one portion to a solution of Fe^{II}aq(BF$_4$)$_2$ (338 mg, 1 mmol) and *tripod* (625 mg, 1 mmol) in 15 mL of acetone. An immediate color change from pale yellow to violet red was observed. After stirring for 5 min at room temperature, a red solid precipitated. This precipitate was isolated by filtration. After dissolving the precipitate in dichloromethane, filtration and evaporation of the dichloromethane gave **3dBF$_4$** as a red-violet microcrystalline solid (460 mg, 48%). Crystals for X-ray diffraction studies were grown by layering a concentrated solution of **3dBF$_4$** in dichloromethane with acetone at −20 °C. For analytical data of **3dBF$_4$** see Tables 1, 2 and 4.

[(*tripod*Fe)$_3${μ-NCC(R)CN}$_3${μ-CN}$_3$Fe−NCC(R)CN]BF$_4$ [5BF$_4$: R = SO_2CH_3 (5aBF$_4$), $COCH_3$ (5bBF$_4$), CO_2CH_3 (5cBF$_4$)] and [(*tripod*Fe)$_3${μ-NCNCN}$_3${μ-CN}$_3$Fe−NCNCN]BF$_4$ (6BF$_4$): Na1a, **Na1a**, **Na1c** or **Na2** (1 mmol) and sodium cyanide (49 mg, 1 mmol) were added, in one portion, to a solution of Fe^{II}aq(BF$_4$)$_2$ (338 mg, 1 mmol) and *tripod* (625 mg, 1 mmol) in dichloromethane/ethanol (1:1; 40 mL). An immediate color change from pale yellow to red was observed. After stirring for 10 h at room temperature the color had changed to orange-red. After stirring for an additional period of 10 h, the resulting turbid orange to red solution was concentrated in vacuo to a volume of 10 mL and filtered. The orange to red precipitate was washed with ethanol and diethyl ether and dried in vacuo. Filtration with dichloromethane through 1 cm of Kieselgur and concentration of the red filtrate yielded the products as orange to red solids. The products were recrystallized from dichloromethane/ethanol yielding the compounds as orange to red crystallized solids. Yields: **5aBF$_4$** (50%), **5bBF$_4$** (38%), **5cBF$_4$** (51%), **6BF$_4$** (46%). For analytical and spectroscopic data of compounds **5aBF$_4$**, **5bBF$_4$**, **5cBF$_4$** and **6BF$_4$** see Tables 3 and 4.

Table 5. Crystallographic data of compounds **3aBF$_4$**, **3bBF$_4$** and **3dBF$_4$**

Compound	**3aBF$_4$**	**3bBF$_4$** [a]	**3dBF$_4$** [b]
Solvate	·0.6 CH_3NO_2·1 $C_4H_8O_2$	·2.5 CH_2Cl_2·1 C_2H_5OH	·0.8 C_3H_6O
Empirical formula (without solvate)	$C_{94}H_{87}BF_4Fe_2N_6O_6P_6S_3$	$C_{97}H_{87}BF_4Fe_2N_6O_3P_6$	$C_{100}H_{81}BF_4Fe_2N_{12}P_6$
Molecular mass [g/mol]	1877.3	1769.1	1835.2
Crystal size [mm]	0.20×0.10×0.05	0.02×0.02×0.03	0.25×0.25×0.25
Crystal system	triclinic	monoclinic	orthorhombic
Space group	$P\bar{1}$	$P2_1/a$	$P2_12_12$
a [pm]	1305.8(3)	1478.5(3)	2045.0(4)
b [pm]	2001.9(4)	4317.2(9)	2088.3(4)
c [pm]	2077.8(4)	1624.2(3)	1313.2(3)
α [°]	110.36(3)	90	90
β [°]	93.77(3)	95.89(3)	90
γ [°]	93.73(3)	90	90
V [10^{6}pm^3]	5058.50	10312.00	5608.10
Z	2	4	2
d_x [g·cm^{-3}]	1.355	1.309	1.114
T [K]	200	200	263
Scan range	3.1° ≤ 2θ ≤ 50.0°	2.5° ≤ 2θ ≤ 54.0°	3.7° ≤ 2θ ≤ 50.0°
Method	ω-scan, Δω =1.0°	ω-scan, Δω =1.0°	ω-scan, Δω =1.0°
Scan speed	25 s/frame	10 s/frame	5 s/frame
No. of measured rflns.	79811	40321	50449
No. of unique rflns.	17826	22346	9890
No. of observed rflns.	10433	13337	7862
Observation criterion	$I \geq 2\sigma$	$I \geq 2\sigma$	$I \geq 2\sigma$
No. of param. refined	998	1156	609
Resid. el. dens. [10^{-6} e·pm^{-3}]	2.18	1.79	0.68
R_1/R_w (%) (refinement on F^2)	7.6/21.9	12.0/39.1	6.7/21.6

[a] The quality of the analysis achieved for **3bBF$_4$** is reduced by the fact, that the crystal contains solvent molecules in disordered arrangements. In addition, there is suspicion, that there is some rotational disorder of the acetyl substituents, which could, however, not be resolved by the split-atom technique. The rotational position, which at least dominates by far is shown in Figure 1. − [b] The solution of the structure of **3dBF$_4$** is as well affected by disorder problems. **3dBF$_4$** is bound to have crystallographic C_2 symmetry, such that there is disorder for the C(CN)$_2$H group, whose central carbon atom lies at the C_2 axis. The disorder was not completely resolved.

Table 6. Crystallographic data of compounds **5aBF$_4$**, **5eBF$_4$** and **5fBF$_4$**

Compound	**5aBF$_4$** [a]	**5eBF$_4$** [b]	**5fBF$_4$** [c]
Solvate	·1.5 CH_3NO_2·2.2 $C_4H_8O_2$	·1.5 CH_3NO_2·1.5 $C_4H_{10}O$	·0.75 H_2O
Empirical formula (without solvate)	$C_{142}H_{129}BF_4Fe_4N_{11}O_8P_9S_4$	$C_{141}H_{117}BF_5Fe_4N_{12}O_3P_9$	$C_{135}H_{117}BClF_4Fe_4N_{12}O_3P_9$
Molecular mass [g/mol]	2834.9	2635.5	2579.9
Crystal size [mm]	0.02×0.02×0.02	0.01×0.01×0.01	0.20×0.20×0.20
Crystal system	monoclinic	cubic	cubic
Space group	$P2_1/n$	$P\bar{4}3n$	$P\bar{4}3n$
a [pm]	1697.22(3)	3308.5(4)	3327.2(4)
b [pm]	3619.06(5)	3308.5(4)	3327.2(4)
c [pm]	2746.04(1)	3308.5(4)	3327.2(4)
α [°]	90	90	90
β [°]	96.851(1)	90	90
γ [°]	90	90	90
V [10^6pm^3]	16746.70	36215.00	36833.00
Z	4	8	8
d_x [g·cm^{-3}]	1.302	1.033	0.934
T [K]	200	253	260
Scan range	2.3° ≤ 2θ ≤ 56.6°	2.5° ≤ 2θ ≤ 52.7°	2.4° ≤ 2θ ≤ 48.0°
Method	ω-scan, Δω =1.0°	ω-scan, Δω =1.0°	ω-scan, Δω =1.0°
Scan speed	10 s/frame	10 s/frame	20 s/frame
No. of measured rflns.	167031	24764	21708
No. of unique rflns.	40222	12384	9659
No. of observed rflns.	17384	5497	6182
Observation criterion	$I \geq 2\sigma$	$I \geq 2\sigma$	$I \geq 2\sigma$
No. of param. refined	1838	552	505
Resid. el. dens. [10^{-6} e·pm^{-3}]	1.82	1.59	1.05
R_1/R_w (%) (refinement on F^2)	11.6/32.1	10.2/34.2	11.1/34.1

[a] The data for X-ray analysis of **5aBF$_4$** were collected with a Siemens SMART 1000-CCD diffractometer. Lorentz, polarisation and absorption correction (Siemens Area Detector Absorption Correction, Siemens) were carried out. – [b] The structure is affected by disorder. The apical ligand is fluoride in the analyzed sample instead of **1e**$^-$, which is present in the bulk (Table 3). – [c] Disorder of solvate and rotational disorder of the substituents of the bridging ligands.

[(*tripod*Fe)$_3${μ-NCC[C(O)CN]CN}$_3${μ-CN}$_3$Fe–NCC-[C(O)CN]CN]BF$_4$ (5eBF$_4$) and [(*tripod*Fe)$_3${μ-NCC(NO)CN}$_3${μ-CN}$_3$Fe–Cl]BF$_4$ (5fBF$_4$): [N(CH$_3$)$_4$]1e and **Na1f** (1 mmol) and sodium cyanide (49 mg, 1 mmol) were added in one portion to a solution of $Fe^{II}aq(BF_4)_2$ (338 mg, 1 mmol) and *tripod* (625 mg, 1 mmol) in dichloromethane/ethanol (1:1; 40 mL). An immediate color change from pale yellow to violet red was observed. After stirring for 10 h at room temperature, a red precipitate had formed. Stirring for an additional period of 10 h, followed by isolation of the red precipitate, filtration with nitromethane through 1 cm of silica gel (ICN Biomedicals, 32–63 μm, 60 Å) and evaporation of the solvent, yielded the products in the form of red solids. Yields: **5eBF$_4$** (67%), **5fBF$_4$** (62%). For purification, the products were crystallized by vapor phase diffusion of diethyl ether into dilute nitromethane solutions. For analytical data of compounds **5eBF$_4$** and **5fBF$_4$** see Tables 3 and 4.

[(*tripod*Fe)$_3${μ-NCC[CH(CN)$_2$]CN}$_3${μ-CN}$_3$FeCN]BF$_4$ (5dBF$_4$) and [(*tripod*Fe)$_3${μ-NCC[CH(CN)$_2$]CN}$_3${μ-CN}$_3$FeCN]PF$_6$ (5dPF$_6$). – Method A: H1d (98 mg, 0.75 mmol), sodium bicarbonate (64 mg, 0.80 mmol) and sodium cyanide (49 mg, 1 mmol) were added in one portion to a solution of $Fe^{II}aq(BF_4)_2$ (338 mg, 1 mmol) and *tripod* (625 mg, 1 mmol) in dichloromethane/ethanol (1:1; 40 mL). An immediate change of color from pale yellow to violet red was observed. After stirring for 10 h at room temperature, an orange red precipitate had formed. Stirring for an additional period of 10 h, followed by isolation of the red precipitate, filtration with nitromethane through 1 cm of Kieselgel (ICN Biomedicals, 32–63 μm, 60 Å) and concentration of the filtrate, yielded **5dBF$_4$** in the form of an orange-brown microcrystalline solid (250 mg, 37%). For purification, the product was recrystallized by vapor phase diffusion of diethyl ether into a concentrated nitromethane/dichloromethane solution of the crude product in an almost quantitative yield. – **Method B:** A solution of **3dBF$_4$** (1700 mg, 0.93 mmol) in dichloromethane/ethanol (1:1; 70 mL) was heated to reflux. After heating for 2 h, the color of the reaction mixture had changed from violet-red to dark-brown. After 10 h of heating, the ν_{CN} absorptions of **3dBF$_4$** had completely disappeared. The mixture was cooled to room temperature, the solvent was evaporated in vacuo and the residue was purified by chromatography on silica gel (ICN Biomedicals, 32–63 μm, 60 Å). Gradually changing the solvent polarity from dichloromethane to dichloromethane/nitromethane (1:1) **5dBF$_4$** was eluted as a brown-red band. After drying in vacuo, 850 mg (70%) **5dBF$_4$** was obtained as a brown solid. Further purification by recrystallization from dichloromethane/ethanol yielded 510 mg (41%) of violet-red hexagonal and cube-shaped crystals of **5dBF$_4$**. – **Method C:** A solution of NaTCNE (227 mg, 1.5 mmol) and sodium hexafluorophosphate (218 mg, 1.3 mmol) in 30 mL of ethanol was added to a suspension of $FeCl_2$ (338 mg, 1 mmol) and *tripod* (625 mg, 1 mmol) in 30 mL of dichloromethane. Stirring of the dark solution for 20 h at room temperature resulted in the formation of a brown-red precipitate, which was isolated, extracted with nitromethane and filtered through 1 cm of silica gel (ICN Biomedicals, 32–63 μm, 60 Å). Evaporation of the solvent from the filtrate left 455 mg (68%) **5dPF$_6$** as a brown solid. For purification, this product was recrystallized by vapor phase diffusion of diethyl ether into a concentrated nitromethane/dichloromethane solution of the crude product giving 370 mg (55%) of violet cube-shaped

Table 7. Crystallographic data of compounds **5dBF$_4$** and **5dPF$_6$** with ligands derived from TCNE

Compound	**5dBF$_4$** [a]	**5dBF$_4$** [b]	**5dPF$_6$** [b] [c]
Solvate	·1.5 H_2O·1.5 C_2H_5OH	·2.1 CH_2Cl_2·4.5 H_2O	·1.5 CH_3NO_2·1.5 C_2H_5OH
Empirical formula (without solvate)	$C_{143}H_{122}BF_4Fe_4N_{14}P_9$	$C_{141}H_{124}BF_4Fe_4N_{12}OP_9$	$C_{141}H_{123}ClF_6Fe_4N_{12}P_{10}$
Molecular mass [g/mol]	2625.6	2591.6	2668.2
Crystal size [mm]	0.20×0.25×0.20	0.40×0.30×0.20	0.30×0.30×0.30
Crystal system	cubic	hexagonal	trigonal
Space group	$P\bar{4}3n$	$P31c$	$P31c$
a [pm]	3278.8(3)	1909.3(3)	1911.8(3)
b [pm]	3278.8(3)	1909.3(3)	1911.8(3)
c [pm]	3278.8(3)	2418.5(5)	2434.5(2)
α [°]	90	90	90
β [°]	90	90	90
γ [°]	90	120	120
V [10^6pm^3]	35247.6(58)	7635.00	7705.9(18)
Z	8	2	2
d_x [g·cm^{-3}]	1.013	1.231	1.218
T [K]	293	200	200
Scan range	2.8° ≤ 2θ ≤ 46.5°	3.0° ≤ 2θ ≤ 52. 0°	2.5° ≤ 2θ ≤ 50.1°
Method	ω-scan, Δω =1.0°	ω-scan, Δω =1.0°	ω-scan, Δω =0.54°
Scan speed	10 s/frame	10 s/frame	12°/min
No. of measured rflns.	16198	26051	9130
No. of unique rflns.	8469	9514	4777
No. of observed rflns.	6370	8091	3344
Observation criterion	$I \geq 2\sigma$	$I \geq 2\sigma$	$I \geq 2\sigma$
No. of param. refined	590	541	420
Resid. el. dens. [10^{-6} e·pm^{-3}]	1.13	1.48	2.07
R_1/R_w (%) (refinement on F^2)	8.7/25.3	8.0/23.4	10.9/25.5

[a] The counterion BF_4^- is replaced by CN^- in about 50 % of the molecules within the crystal. The $CH(CN)_2$ substituent is exchanged by a CH_2CN group in 65 % of the molecules. – [b] The substituents at the bridging dicyanomethanide units are found to be CH_2CN groups. – [c] Data for **5dPF$_6$** were collected with a Siemens (Nicolet synthex) R3m/V diffractometer.

crystals of **5dPF$_6$**. Analytical and spectroscopic data of compound **5dBF$_4$** are listed in Tables 3 and 4.

X-ray Crystallographic Study: Suitable crystals were taken directly out of the mother liquor, immersed in perfluorinated polyether oil and fixed to a glass capillary. The measurements were carried out with a Nonius-Kappa CCD diffractometer (low-temperature unit, graphite-monochromated Mo-K_α radiation), unless stated otherwise. The data were processed by the standard Nonius software.[38] All calculations were performed using the SHELX software package. Structures were solved by direct methods with the program SHELXS-97[39] and refined with the program SHELXL-97.[40] Graphical handling of the structural data during solution and refinement was performed with XPMA.[41] Atomic coordinates and anisotropic thermal parameters of the non-hydrogen atoms were refined by full-matrix least-squares calculations. Data for the structure determinations are compiled in Tables 5, 6 and 7. Figures 1 and 3 were prepared using WinRay-32 [42] and WinRay-GL.[43] Crystallographic data (excluding structure factors) for the structures reported in this paper have been deposited with the Cambridge Crystallographic Data Centre as supplementary publication nos. CCDC-156047 to -156055. Copies of the data can be obtained free of charge on application to CCDC, 12 Union Road, Cambridge CB2 1EZ, UK [Fax: (internat.) + 44-1223/336-033; E-mail: deposit@ccdc.cam.ac.uk].

Acknowledgments

We are indebted to the Deutsche Forschungsgemeinschaft and the Fonds der Chemischen Industrie for financial support. The unselfish cooperation of Dr. J. Groß and co-workers of the mass spectrometry department and the workers of the microanalytical laboratory of the Organisch-Chemisches Institut der Universität Heidelberg is gratefully acknowledged. We are indebted to Mr. D. Günauer for the cyclic voltammetric measurements.

[1] S. Mann, G. Huttner, L. Zsolnai, K. Heinze, *Angew. Chem.* **1996**, *108*, 2983; *Angew. Chem. Int. Ed. Engl.* **1996**, *35*, 2808.
[2] H. Heidel, J. Scherer, A. Asam, G. Huttner, O. Walter, L. Zsolnai, *Chem. Ber.* **1995**, *128*, 293.
[3] J.-M. Lehn *Supramolecular Chemistry – Concepts and Perspectives*, VCH, Weinheim, **1995**.
[4] D. L. Caulder, K. N. Raymond, *J. Chem. Soc., Dalton Trans.* **1999**, 1185.
[5] M. Fujita, *Struct. Bond.* **2000**, *96*, 177.
[6] R. W. Saalfrank, E. Uller, B. Demleitner, I. Berndt, *Struct. Bond.* **2000**, *96*, 149.
[7] B. Olenyuk, A. Fechtenkötter, P. J. Stang, *J. Chem. Soc., Dalton Trans.* **1998**, 1707.
[8] S. Mann, G. Huttner, L. Zsolnai, K. Heinze, V. Jacob, B. Antelmann, A. Driess, B. Schiemenz, *Z. Naturforsch., Teil B* **2000**, *55*, 638.
[9] J. P. Fleury, B. Libis, *Bull. Soc. Chim. Fr.* **1966**, 1966.
[10] R. Dijkstra, H. J. Backer, *Recl. Trav. Chim. Pays-Bas* **1954**, *73*, 569.
[11] H. Köhler, K. Rassmi, H. Skirl, *Z. Allg. Anorg. Chem.* **1985**, *529*, 173.
[12] F. Arndt, H. Scholz, E. Frobel, *Justus Liebigs Ann. Chem.* **1936**, *521*, 95.
[13] J. A. Elvidge, P. N. Judson, A. Percival, R. Shah, *J. Chem. Soc., Perkin Trans. 1* **1983**, 1741.

[14] W. J. Middleton, R. E. Heckert, E. L. Little, C. G. Krespan, *J. Am. Chem. Soc.* **1958**, *80*, 2783.
[15] W. J. Middleton, E. L. Little, D. D. Coffman, V. A. Engelhardt, *J. Am. Chem. Soc.* **1958**, *80*, 2795.
[16] H. Köhler, G. Lux, *Inorg. Nucl. Chem. Lett.* **1968**, *4*, 133.
[17] The anion derived from **H1d** upon monodeprotonation has been studied: O. E. Nasakin, E. G. Nikolaev, P. B. Terent'ev, V. D. Sheludyakov, *J. Org. Chem. USSR (Engl. Transl.)* **1987**, *23*, 597.
[18] A. G. Sharpe *The Chemistry of Cyano Complexes of the Transition Metals*, Academic Press, New York, **1976**.
[19] L. Jäger, B. Freude, A. Krug, H. Hartung, *J. Organomet. Chem.* **1994**, *467*, 163.
[20]]L. Jäger, B. Freude, R. Skirl, H. Köhler, *Z. Allg. Anorg. Chem.* **1993**, *619*, 711.
[21] V. Jacob, G. Huttner, E. Kaifer, P. Kircher, *Z. Naturforsch.*, in press
[22] T. C. Gibb, N. N. Greenwood, *J. Chem. Soc.* **1965**, 6989.
[23] P. R. Edwards, C. E. Johnson, R. J. P. Williams, *J. Chem. Phys.* **1967**, *47*, 2074.
[24] G. M. Bancroft, J. M. Dubery, *J. Chem. Phys.* **1969**, *50*, 2264.
[25] F. A. Cotton, C. A. Murillo, D. F. Timmons, *Polyhedron* **1999**, *18*, 423.
[26] R. S. Drago *Physical Methods in Inorganic Chemistry*, 2ed., Saunders, Philadelphia, **1992**.
[27] O. W. Webster, W. Mahler, R. E. Benson, *J. Org. Chem.* **1960**, *25*, 1470.
[28] O. W. Webster, W. Mahler, R. E. Benson, *J. Am. Chem. Soc.* **1962**, *84*, 3678.
[29] C. Creutz, *Prog. Inorg. Chem.* **1983**, *30*, 1.
[30] J. E. Sutton, P. M. Sutton, H. Taube, *Inorg. Chem.* **1979**, *18*, 1017.
[31] H. Krenzien, H. Taube, *J. Am. Chem. Soc.* **1976**, *98*, 6379.
[32] H. Krenzien, H. Taube, *Inorg. Chem.* **1982**, *21*, 4001.
[33] A. Asam, B. Janssen, G. Huttner, L. Zsolnai, O. Walter, *Z. Naturforsch., Teil B* **1993**, *48*, 1707.
[34] *Organikum*, Deutscher Verlag der Wissenschaften, Berlin, **1990**,
[35] W. Hewertson, H. R. Watson, *J. Chem. Soc.* **1962**, 1490.
[36] A. Muth, O. Walter, G. Huttner, A. Asam, L. Zsolnai, C. Emmerich, *Z. Naturforsch., Teil B* **1994**, *49*, 149.
[37] H. Funk, F. Binder, *Z. Anorg. Allg. Chem.* **1926**, *155*, 327.
[38] *DENZO-SMN*, Data processing software, Nonius **1998**; http://www.nonius.com
[39] G. M. Sheldrick, *SHELXS-97*, Program for Crystal Structure Solution, University of Göttingen, **1997**; http://shelx. uni-ac. gwdg. de/shelx/index. html
[40] G. M. Sheldrick, *SHELXL-97*, Program for Crystal Structure Refinement, University of Göttingen, **1997**; http://shelx. uni-ac. gwdg. de/shelx/index. html
[41] L. Zsolnai, G. Huttner, *XPMA*, University of Heidelberg, **1994**; http://www.uni-heidelberg.de/institute/fak12/AC/huttner/htmlsoftware. html
[42] R. Soltek, G. Huttner, *WinRay-32*, University of Heidelberg, **1998**; http://www.uni-heidelberg.de/institute/fak12/AC/huttner/htmlsoftware.html
[43] R. Soltek, G. Huttner, *WinRay-GL*, University of Heidelberg, **2000**; http://www.uni-heidelberg.de/institute/fak12/AC/huttner/htmlsoftware.html.

Received February 16, 2001
[I01056]